



Development of electroresponsive functional soft materials by electroresponsive dopants

Yoshimitsu Itoh ^{1,2} · Daiki Morishita¹

Received: 18 April 2023 / Revised: 19 May 2023 / Accepted: 22 May 2023 / Published online: 23 June 2023

© The Author(s) 2023. This article is published with open access

Abstract

In this Focus Review, we summarize our new strategy to create electroresponsive soft materials using electroresponsive dopants. Liquid crystals (LCs) are representative electroresponsive soft functional materials that have been utilized for various applications, including LC display devices. The response to the applied electric field (E-field) is generally realized by the direct coupling between the E-field and the LC molecules. Thus, LC molecules must simultaneously exhibit electroresponsiveness and LC properties. As a new concept to create electroresponsive soft materials, we came up with an idea of using electroresponsive dopants. Dopants can change the property of the LC material only with a minute amount and do not need to have an LC property by itself, thus allows more freedom for the molecular design. Based on this new concept, we developed several intriguing materials, such as cholesteric displays with rewritable color memory functions and quick color modulation functions, which are both unprecedented. We also utilized this concept to columnar LC systems and realized multiresponsive columnar LC materials, which are usually rigid and poorly responsive to applied external perturbations.

Introduction

Liquid crystal (LC) is among the most representative electroresponsive soft materials [1, 2]. For example, typical LC display devices utilize rod-shaped nematic LC molecules that tend to align parallel to each other and switch macroscopic orientations in response to an applied electric field (E-field) to control the transmission of light [3, 4]. This response is realized by the coupling between the E-field and the LC molecules. The LC molecules need a preinstalled E-field-responsive molecular unit. However, designing new E-field responsive LC molecules is not easy. This is because the emergence of the LC property is largely governed by the “shape” of the molecule, and the E-field-responsive molecular unit is not always compatible with

this principle. In our group, we employed a different strategy to create new E-field responsive soft materials. We focused on a “dopant” (Fig. 1). A dopant in LC materials is a compound that can largely change the properties of the LC material when a small amount is added. One of the most representative examples is cholesteric LCs [5, 6]. When a chiral dopant is added to a nematic LC, macroscopic helical molecular ordering of several hundred to thousands of nanometers emerges while maintaining the nanoscale parallel molecular arrangement. As a result, a wavelength of light that corresponds to the helical pitch is reflected, and bright reflection color becomes visible. The amount of the dopant is generally smaller than that of the host LC molecules; thus, the dopant can be called a “catalyst” that changes the properties of LC materials. Our strategy for developing novel electroresponsive materials is to couple the E-field to the dopant rather than the host LC molecules. As the amount of dopant necessary is only “catalytic”, the only requirement for the dopant is the minimum solubility to the host LC material. Generally, there is no strong obligation for the molecular shape. Therefore, a variety of molecular designs and E-field responsiveness have become possible. In this Focus Review, we introduce several electroresponsive materials that were developed in our group based on this concept.

✉ Yoshimitsu Itoh
itoh@chembio.t.u-tokyo.ac.jp

¹ Department of Chemistry and Biotechnology, School of Engineering, The University of Tokyo, 7-3-1 Hongo, Bunkyo-ku, Tokyo 113-8656, Japan

² Japan Science and Technology Agency (JST), Precursory Research for Embryonic Science and Technology (PRESTO), 4-1-8 Honcho, Kawaguchi, Saitama 332-0012, Japan

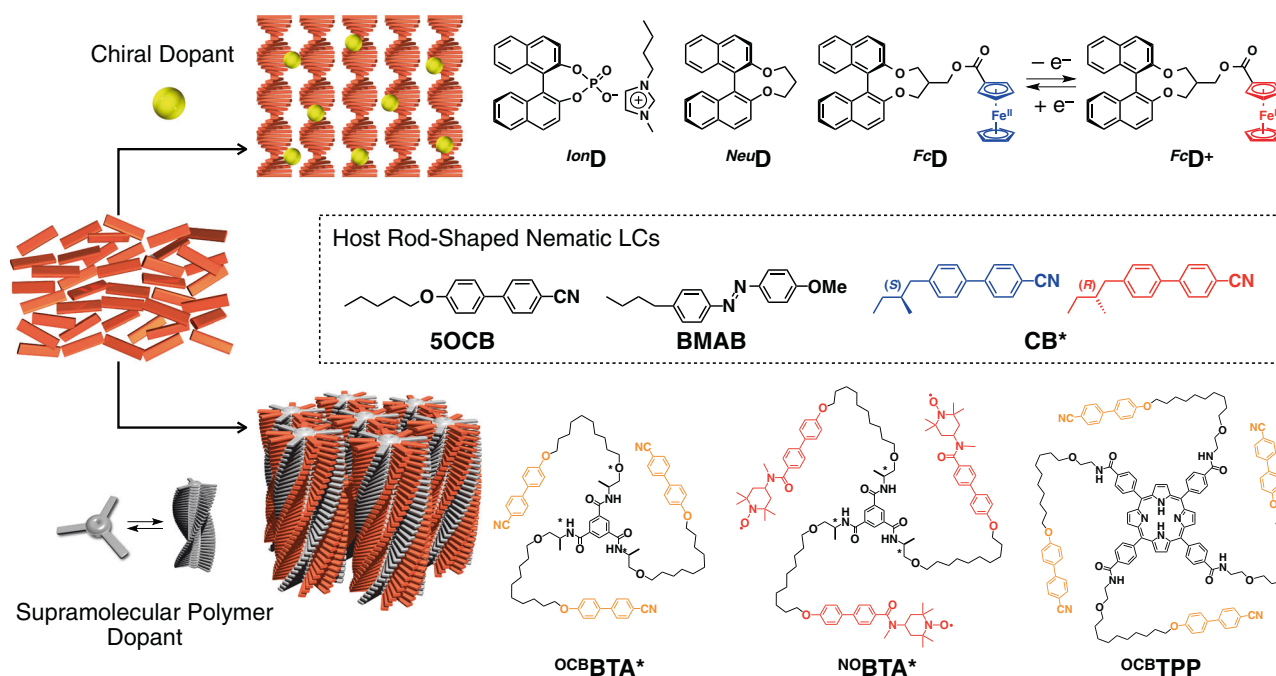


Fig. 1 Schematic representations of electroresponsive functional soft materials by electroresponsive dopants, together with the molecular structures utilized for the realization of these materials

Electroresponsive chiral dopant for color-modulable cholesteric LC

The first LC compound discovered by Friedrich Reinitzer in 1888 was a cholesterol derivative [7, 8]. These molecules organize themselves into a macroscopic helical geometry in their LC phase, which is called the cholesteric phase or chiral nematic phase. The most characteristic feature of cholesteric LCs is selective reflection due to internal helical ordering. The reflection wavelength (λ) is determined by the helical pitch (P) as follows:

$$\lambda = nP \quad (1)$$

where n is the average refractive index of the LC. When the wavelength and the corresponding helical pitch fall into the range of the visible region, a bright reflection color can be observed. Meanwhile, the cholesteric phase is formed not only from the cholesterol derivative but also from a nematic LC doped with a chiral molecule (dopant). In such a case, the reflection wavelength of the cholesteric LCs is determined as follows:

$$\lambda = nP = n/\beta_M \cdot C \quad (2)$$

where β_M is the helical twisting power based on a molar fraction of the dopant (HTP; μm^{-1}) and C is the molar concentration of the dopant.

For the application of cholesteric LCs to display devices, we need to endow the LCs with electrical responsiveness. Cholesteric LCs can change the direction of the internal

helical axis in response to an applied electric field (E-field) [9, 10]. When the helical axis is perpendicular to the substrate surface (planer state), a specific wavelength of light (λ) will be reflected as described above (selective reflection). When the helical axis is randomly oriented (focal conic state), the incident light will be scattered, and the device will look opaque. These two states can be reversibly switched using an E-field, and each state can be maintained even after the removal of the E-field. This bistability is applicable to electronic paper (E-paper) [11, 12]. However, this system can only switch the reflection on and off but cannot change the color of the LC device.

To change the reflection color of the cholesteric LC devices, the helical pitch must be changed by electrical stimuli. However, this method is known to be difficult. In the earliest example, a dedicated electrical cell was utilized for the display device, which can apply an E-field perpendicular to the helical axis [13]. In this way, the constituent polar rod-shaped molecule is forced to align parallel to the E-field. Accordingly, the helical pitch will be expanded to shift the reflection wavelength to a longer wavelength region. This method not only requires a dedicated cell but also a voltage above 100 V. Additionally, this device cannot realize a color shift in the visible wavelength region. The other method is to utilize a molecule where the molecular dipole is perpendicular to the long axis of the molecule (negative dielectric anisotropy) [10, 14, 15]. Cholesteric LCs obtained using such molecules can tilt the helical axis in response to the applied voltage (>40 V) [10]. However, because each domain has a

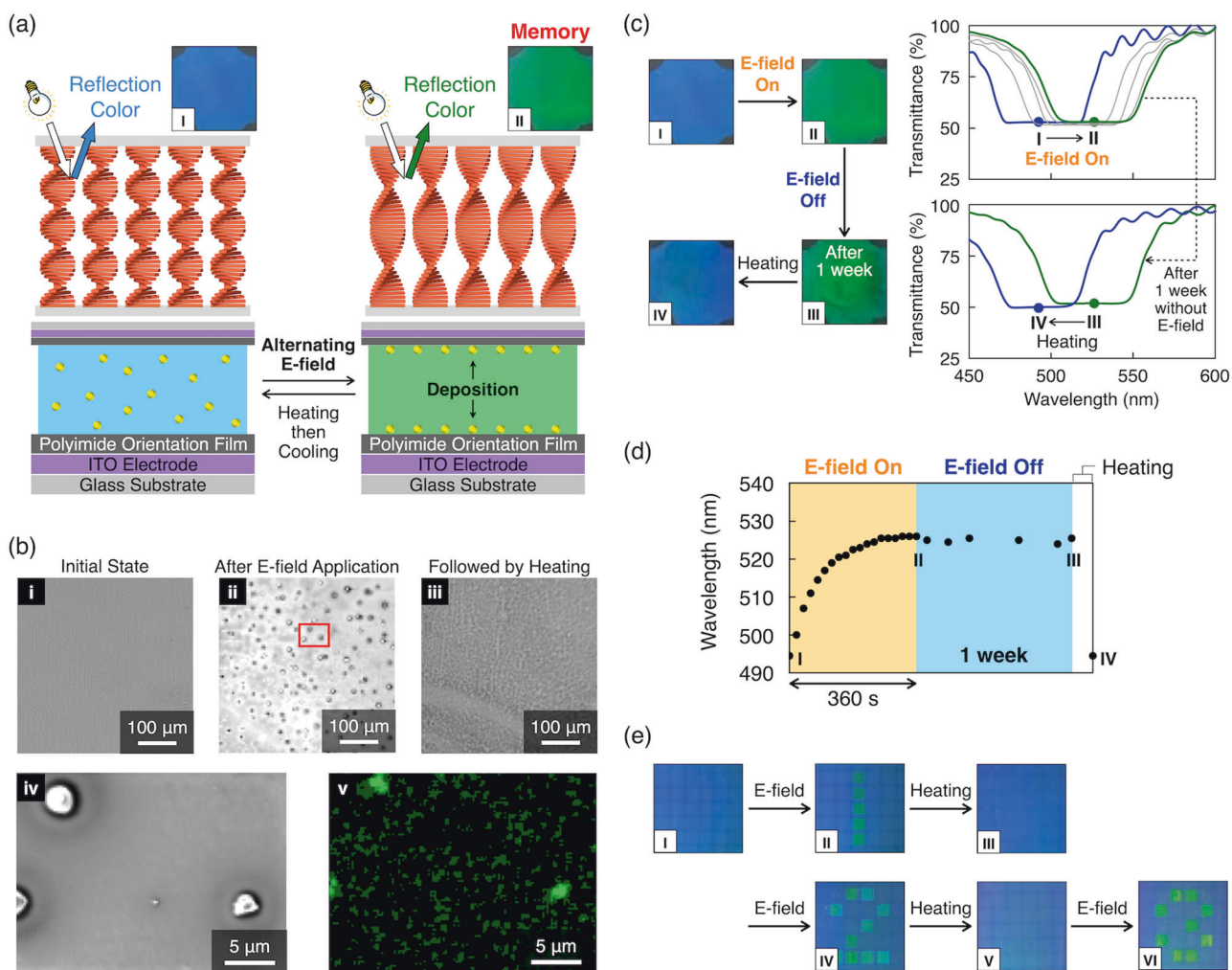


Fig. 2 **a** Schematic representation of the mechanism behind the reflection color change by EPD of ^{lon}D . Pictures I and II show a center part of the device before and after the E-field application, respectively. The final color was induced by heating the device to an isotropic temperature followed by cooling to generate a cholesteric phase. **b** Deposition of particles composed of ionic chiral dopant ^{lon}D at the electrode surfaces. (i–iii) SEM images of the electrode surfaces derived from the devices, (i) in the initial state, (ii) after E-field application (40 Vpp, 100 Hz for 360 s), and (iii) followed by heating (80 °C for 24 h). (iv) Enlarged SEM image of the deposited material in the red square in (ii). (v) SEM-EDX mapping of phosphorous in (iv). **c** Memory of E-field-modulated reflection colors. The initial blue color (picture I and transmittance spectrum I) changed to green (picture II and

transmittance spectrum II) upon application of an E-field (40 Vpp, 100 Hz) for 0, 60, 120, 240, and 360 s. The E-field was turned off whenever each spectrum was measured. The color remained unchanged for 1 week at 45 °C after the E-field was removed (picture III and transmittance spectrum III). After the device was subsequently heated at 80 °C for 24 h, the color reverted to its initial state (picture IV and transmittance spectrum IV). Pictures of a cholesteric LC device were taken at 45 °C. **d** Time-dependent transmittance spectral changes at the center wavelength of the reflection band before and after turning off the E-field application. **e** A cholesteric LC display device utilizing a simple 8 × 8 matrix cell. Reproduced from [19] with permission (Copyright: 2016 Wiley-VCH)

different tilting angle, the tilting orientation can be different by the LC domains; thus, the interference of light scattering with the reflection color is likely unavoidable. The use of a command surface is also reported to change the reflection color of cholesteric LCs [16, 17].

Before our work, nearly all previous approaches for the electrical modulation of cholesteric reflection color were based on a design principle that involves perturbing the arrangement of host LC molecules by directly controlling the LC molecules. On the other hand, we focused on

electrically modulating the properties of the chiral dopant to change the cholesteric reflection color (Figs. 2 and 3). The only example of this approach is the use of ferroelectric LC as a dopant for cholesteric LCs [18]. To date, we have succeeded in developing two kinds of electroresponsive chiral dopants. One can change its concentration within the host LC molecules (Generation 1: ^{lon}D , Fig. 2) [19]. Due to this dopant, the electrically modulated reflection color can be memorized, which can recover its original color simply by heating. This bistable color modulation was realized for

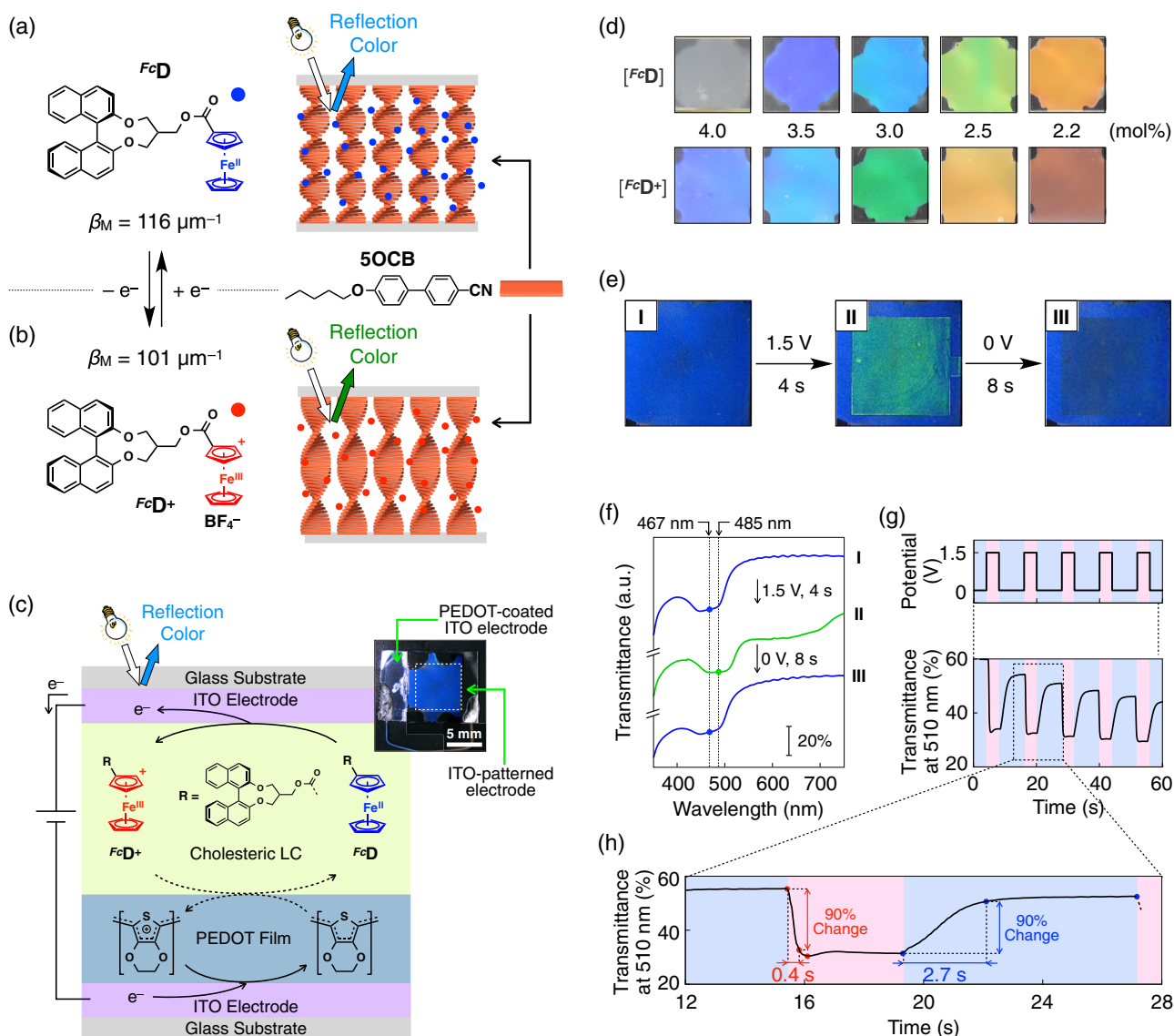


Fig. 3 Chemical structures of **a** ferrocene-appended chiral dopant FcD and **b** its oxidized form FcD^+ , together with schematic representations of FcD - and FcD^+ -doped cholesteric LCs comprising 5OCB sandwiched between two glass substrates. **c** Schematic representation and photograph (inset) of the FcD -doped cholesteric LC device containing EMIm-OTf in 5OCB. The illustration represents the mechanism of electrochemical modulation of the reflection color. **d** Photographs of FcD - and FcD^+ -doped cholesteric LCs in a sandwich-type glass cell at 37 °C at varying concentrations of FcD and FcD^+ .

the first time. This character can be a good candidate for full-color electronic paper using a single LC cell. The other type of electroresponsive dopant is the redox-responsive dopant, which can change its HTP upon oxidation/reduction (Generation 2: FcD , Fig. 3) [20]. This dopant can realize quick color modulation (<1 s) by the application of a voltage as low as 1.5 V.

The concept of dopant Generation 1 is to utilize electrophoretic deposition to change the concentration of the dopant by electrical stimuli. According to Eq. 2, the change

e Photographs and **f** transmittance spectra of the FcD -doped LC device containing 3.0 mol% EMIm-OTf in 5OCB in its initial state (I) after the application of 1.5 V for 4 s (II), and subsequent application of 0 V for 8 s (III) at 37 °C. **g** Changes in the transmittance of the LC device at 510 nm upon switching the applied voltage between +1.5 and 0 V. **h** Details of the transmittance change of the LC device at 510 nm. Reproduced from [20] with permission (Copyright: 2018 American Chemical Society)

in the concentration of the chiral dopant leads to a change in the reflection color of the cholesteric LC material. Thus, we designed the molecule ^{Ion}D (Fig. 1), which has an imidazolium-based ionic moiety and binaphthyl moiety; this is a well-known framework often employed as a core structure of chiral dopants [6]. This dopant was revealed to exhibit an HTP of $\beta_M = 18 \mu\text{m}^{-1}$. The LC material based on ^{Ion}D (1.1 mol%) contains 4'-pentyloxy-4-cyanobiphenyl (5OCB, Fig. 1), which acts as the host LC, a neutral chiral dopant (^{Neu}D , $\beta_M = 83 \mu\text{m}^{-1}$, 3.4 mol%, Fig. 1) to

compensate for the low HTP of ^{Ion}D for realizing reflection in the visible range. We also added a small amount of acetic acid (1.1 mol%), which was found to enhance the reproducibility and uniformity of the E-field-induced color change. When this LC mixture was introduced to a sandwich-type electrical cell coated with a polyimide orientation film, the LC device exhibited a bright blue reflection color at 45 °C (Fig. 2a, I). The shape of the transmittance spectrum of the LC device (Fig. 2c, I in the right top spectrum) was typical for a cholesteric LC whose bandwidth ($\Delta\lambda$) was 47 nm. This value matched well with the calculated value of 55 nm based on the HTP values of the chiral dopants together with the ordinary ($n_o = 1.53$) and extraordinary ($n_e = 1.71$) refractive indices of **5OCB** at 45 °C. Upon application of an alternating current (AC) E-field at a voltage of 40 V peak-to-peak (V_{pp}) at 100 Hz, the reflection color gradually changed to a longer wavelength region and reached a plateau in 360 s, resulting in the emergence of a green reflection color (Fig. 2a, II). The green color remained unchanged for at least one week (Fig. 2c, d). After the cell was heated at 80 °C for 24 h, the device recovered its original blue reflection color (Fig. 2c, d). Among several previous works on the E-field modulation of cholesteric reflection color, our device is the first to realize rewritable color memory. Our design of the mechanism for this color change was an electrophoretic deposition (EPD) of the ionic chiral dopant ^{Ion}D to the electrode surface (Fig. 2a). Once ^{Ion}D is deposited onto the electrode surface, the effective concentration of ^{Ion}D is significantly reduced, thereby elongating the reflection wavelength according to Eq. 2. In addition, the deposited dopant remains on the electrode surface unless it is redissolved into the host LC again. The mechanism of this color modulation/memorization was clarified by time-of-flight secondary-ion mass spectrometry (TOF-SIMS) and scanning electron microscopy (SEM) with energy dispersive X-ray microanalyzer (EDX) of the electrode surface of the cell, in which the deposited dopant was clearly observed (Fig. 2b). By using a matrix cell, we can write and erase different numbers repeatedly (Fig. 2e).

The difference between chiral dopant Generation 1 (^{Ion}D) and Generation 2 (^{Fc}D) is the background mechanism of the color change. According to Eq. 2, the reflection color can be changed by the change in concentration of chiral dopant and change in the HTP (β_M). Although several chiral dopants can change their HTP values upon application of external stimuli [21], mostly using light [22–30], electrical stimuli have never been utilized to change the HTP. During the investigation of chiral dopant Generation 1, we noticed that ionic chiral dopants tend to exhibit lower HTP values than those of neutral dopants. From this observation, we decided to introduce redox-responsive units as a part of the chemical structure of chiral dopants, as redox-responsive units can

change their ionicity upon reduction or oxidation. Thus, we designed ^{Fc}D (Fig. 1), in which the redox-responsive ferrocene (Fc) unit was introduced to the binaphthyl unit. When ^{Fc}D (3.0 mol%, Fig. 1) was mixed with **5OCB** (Fig. 1) and introduced into a sandwich cell, the material exhibited a blue reflection color centered at 479 nm (Fig. 3d, top, 3.0 mol%). When we chemically oxidized ^{Fc}D with $NOBF_4$ to generate $^{Fc}D^+$, the reflection color changed to green ($\lambda = 530$ nm) (Fig. 3d, bottom, 3.0 mol%). By measuring the reflection wavelength at various concentrations of ^{Fc}D (Fig. 3d), we determined the HTP values (β_M) of ^{Fc}D and $^{Fc}D^+$ to be 116 and 101 μm^{-1} , respectively (Fig. 3a, b). These results strongly support our hypothesis that ionic chiral dopants show lower HTP values than those of their neutral counterpart. To realize the redox-responsive color change, we need to consider several factors. The first step is to introduce an electrolyte to enhance the redox reaction within the LC mixture, as electrochemical reactions are promoted in the presence of an electrolyte [31]. Thus, we employed 1-ethyl-3-methylimidazolium trifluoromethanesulfonate (**EMIm-OTf**) (3.0 mol%). The second point is the counter redox couple. When oxidation of ^{Fc}D occurred at one side of the electrode, another component had to be reduced at the other electrode. For this purpose, we fabricated a PEDOT film on one side of the electrode (Fig. 3c) [32]. After 1.5 V was applied to the LC device using 3.1 mol% ^{Fc}D in **5OCB**, color modulation from blue to green occurred quickly (Fig. 3e–h). When we measured the time for 90% color change, it was only 0.4 s, which is the fastest among any E-field responsive color-modulable cholesteric LC system. In addition, the color modulation occurred with a 1.5 V dry-cell battery.

Currently, the electroresponsive dopant Generation 1 can achieve color memory, but the color modulation speed is very slow (forward: 6 min (45 °C), backward: 24 h (at 80 °C)), and the necessary voltage is very high (40 V). On the other hand, Generation 2 can realize a quick color change (forward: 0.4 (37 °C), backward: 2.7 s (37 °C)). If we want to achieve a full-color E-paper, both color memory and quick response, which are usually mutually exclusive, must be realized simultaneously. A chiral dopant with multiredox properties could be a solution to realize this function.

Electroresponsive helical supramolecular dopant for dual-responsive columnar LC material

Nematic LCs are known to be quickly alignable by an external E-field, and this character is elegantly utilized in LC display devices, as described above. However, columnar LCs cannot be easily aligned by the E-field. This is due

to their two-dimensional molecular ordering, which is higher than that of one-dimensionally ordered nematic LCs. High molecular ordering leads to high structural integrity and thus leads to high viscosity and low fluidity of the LC material. Although columnar LCs have promising applications for organic electronics, separation membranes, and high-density memory devices due to their capabilities for electron transport, mass transport, and polarization along the columnar axis, respectively, low alignability has always been an issue for developing practical devices out of columnar LCs. In 2011, Aida and his coworkers reported a simple but general approach to this issue [33]. They found that introducing an amide group at the side chain unit of the disk-shaped core is an effective method to confer E-field responsiveness to the resultant columnar LCs. This paper demonstrated the effectiveness of the amide groups to realize a homeotropic alignment of various 1D-stacked π -conjugated discs parallel to the applied E-field [34–36]. However, the responsiveness is not satisfactory; the orientation is achieved by the slow cooling of their isotropic melt to a temperature that shows the LC phase under the application of an E-field. Nevertheless, achieving in situ isothermal orientation of columnar LCs is still difficult.

In 2019, we reported a new columnar LC system that is mainly composed of rod-shaped nematic LC molecules doped with disk-shaped molecules capable of H-bonding-induced supramolecular polymerization [37] (Fig. 4c). Considering that rod-shaped molecules tend to align parallel to each other and disk-shaped molecules tend to stack one-dimensionally, it is difficult to coassemble these two types of molecules. When the polymer-LC affinity is large, it results in the dispersion of the polymer in the LC matrix (Fig. 4b). On the other hand, when the polymer LC affinity is small, macroscopic phase separation occurs (Fig. 4d). In the latter case, the cross-linked network, formed by the insoluble polymer bundles, transformed the LC material into a gel to exhibit interesting physical properties [38]. In our case (Fig. 4c), introducing the mesogenic moiety, similar to that of rod-shaped nematic LC molecules, at the termini of the side chain of the disk-shaped molecules (Fig. 1) was the key to realizing the order-increasing mesophase transition to a columnar phase; the mesogenic moiety functions as a compatibilizing unit for mixing these two molecules. This unusual coassembly system was not discovered through de novo design but by chance. As a continuation of the above-described E-field responsive cholesteric LC devices, we investigated a helical supramolecular polymer as a new chiral dopant. However, when we utilized a chiral benzenetricarboxiamide (BTA) analog appended with a long aliphatic side chain, one of the most commonly utilized chiral monomers for helical supramolecular polymerization through H-bonding interactions, we

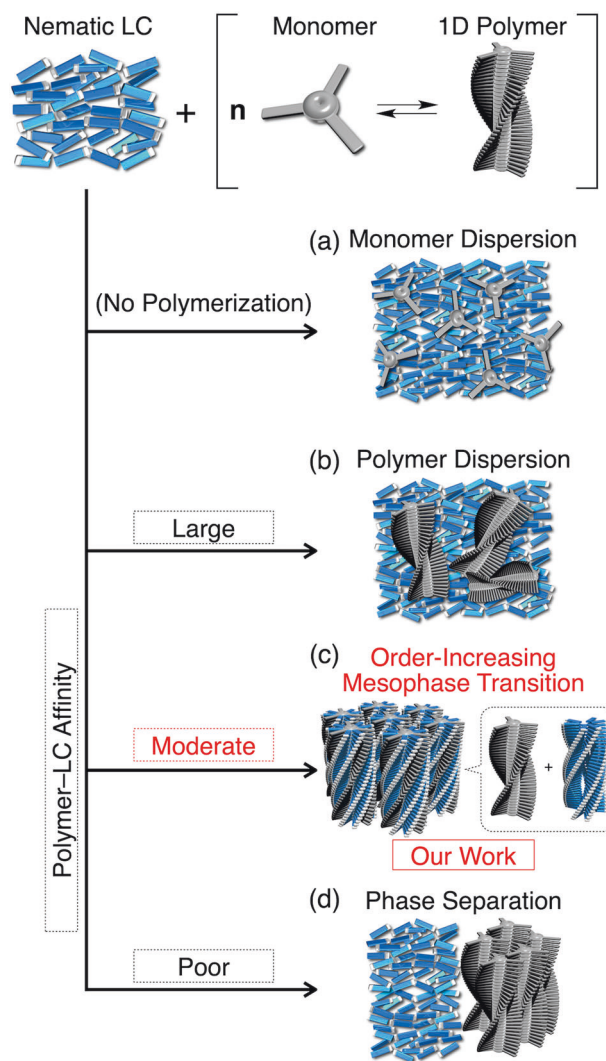


Fig. 4 Schematic representations of possible modes of supramolecular polymerization in LC media. A monomer can form its one-dimensional supramolecular polymer in a nematic LC medium. Depending on the affinity between the monomer or the resultant supramolecular polymer and the LC medium, four different modes are expected: **a** monomer dispersion, **b** polymer dispersion, **c** order-increasing mesophase transition and **d** phase transition. Reproduced from [37] with permission (Copyright: 2019 The American Association for the Advancement of Science)

observed bundled fibers that were phase-separated from the host nematic LC **5OCB** (Fig. 4d). To prevent phase separation, we introduced an oxy-cyanobiphenyl (OCB) moiety at the termini of the aliphatic side chain (^{OCB}BTA) and mixed it with **5OCB** (^{OCB}BTA/**5OCB** = 1/6). This time, the two components were completely miscible. To our surprise, the whole system turned into a columnar rectangular phase upon cooling from its isotropic melt to 100 °C (Fig. 5a, b). This is counterintuitive, as 86 mol% of the LC mixture is composed of rod-shaped **5OCB**, which preferentially aligns parallel to each other to generate a nematic LC phase. After being mixed with ^{OCB}BTA, **5OCB**

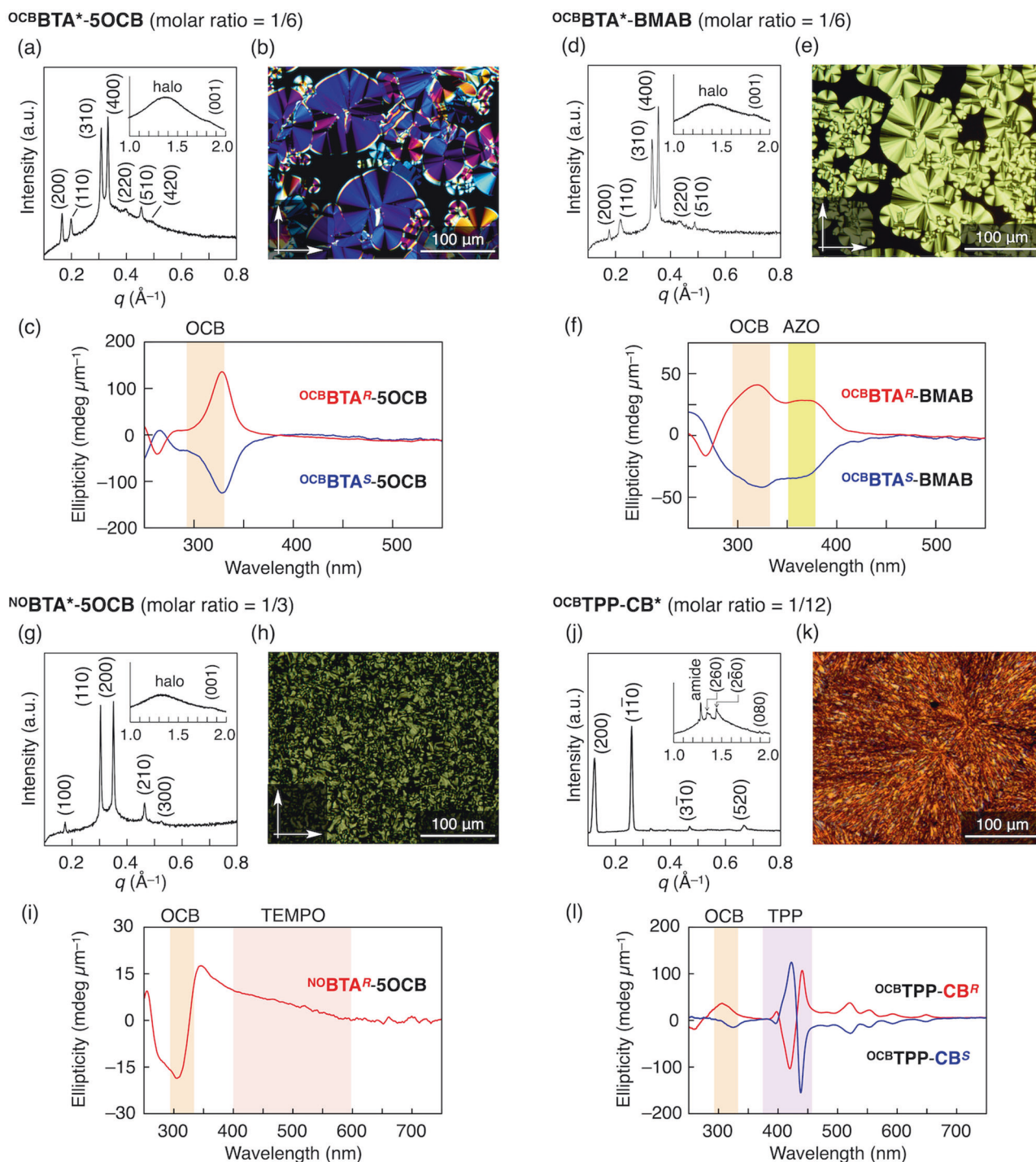


Fig. 5 a, d, g, j XRD profiles, b, e, h, k POM images, and c, f, i, l CD spectra of a–c $\text{OCB}^{\text{BTA}^*}\text{-5OCB}$ (molar ratio = 1/6) at 100 °C, d–f $\text{OCB}^{\text{BTA}^*}\text{-BMAB}$ (molar ratio = 1/6) at 140 °C, g–i $\text{NOBTA}^*\text{-5OCB}$ (molar ratio = 1/3) at 110 °C, and j–l $\text{OCB}^{\text{TPP}}\text{-CB}^*$ (molar

ratio = 1/12) at 40 °C. a–f, g–i, and j–l are reproduced from [37] (Copyright: 2019 American Association for the Advancement of Science) [40], (Copyright: 2019 American Chemical Society) and [47] (Copyright: 2022 Wiley-VCH), respectively, with permission

underwent an order-increasing mesophase transition to a columnar phase (Fig. 4c).

Columnar LC material is composed of columns that are two-dimensionally packed. In our new rod-disk hybrid columnar LC, the individual column has a core-shell

structure in which a helically assembled OCB^{BTA} is surrounded by a helically assembled **5OCB** (Fig. 4c). When looking at the orientation of the functional groups, the amide group is parallel to the columnar axis, while the cyano group is oriented perpendicularly and radially to the

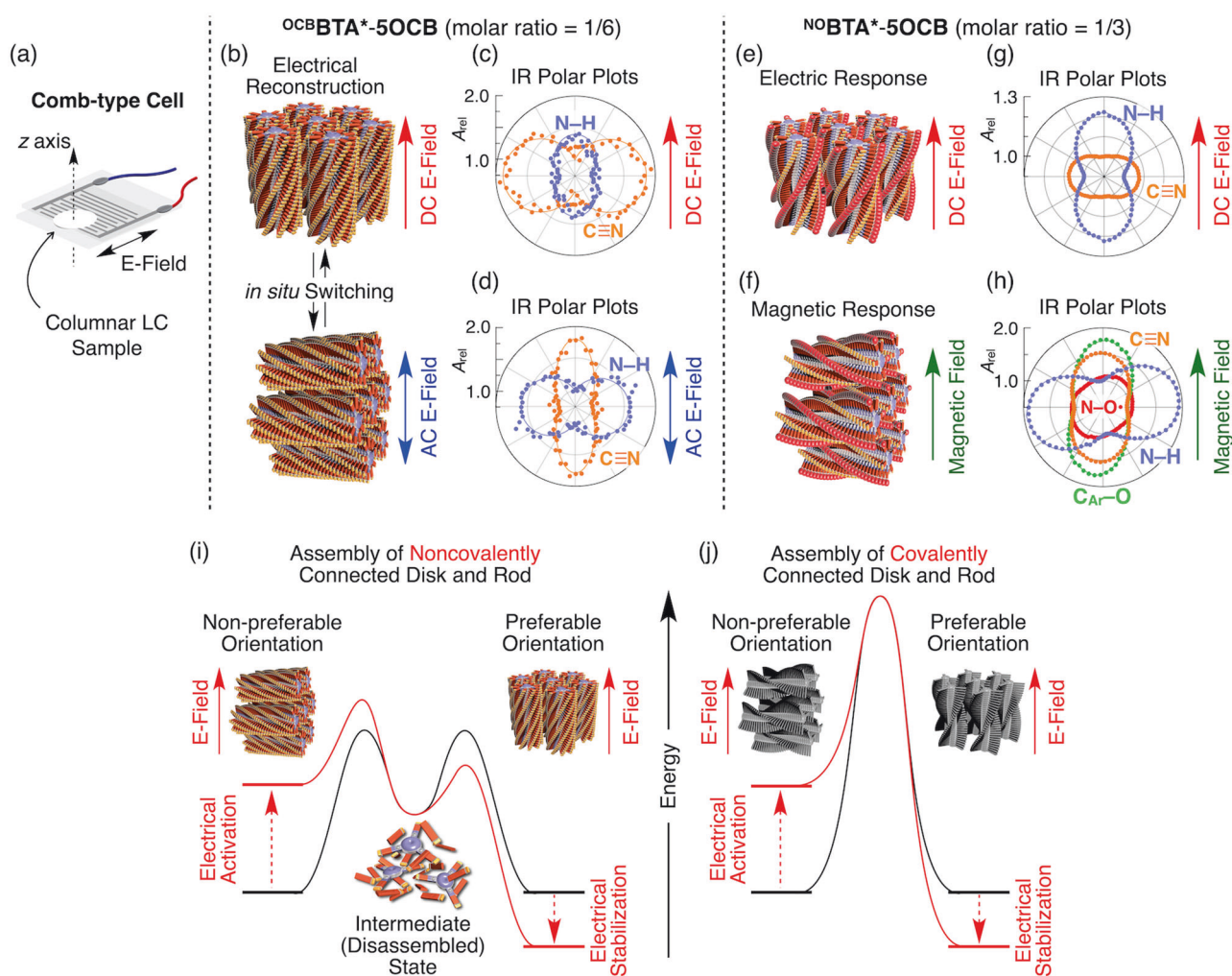


Fig. 6 **a** Schematic representation of a comb-type electrical cell comprising two parallel glass plates ($20\ \mu\text{m}$ of separation) for in-plane E-field application. **b**, **e**, **f** Schematic representations and **c**, **d**, **g**, **h** polar plots of the polarized FT-IR absorption intensities of **b–d** $^{\text{oCBT}}\text{A}^*\text{-5OCB}$ (molar ratio = 1/6) at $100\ ^\circ\text{C}$ and **e–h** $^{\text{nCBT}}\text{A}^*\text{-5OCB}$ (molar ratio = 1/6) at $110\ ^\circ\text{C}$. **b–d** The sample was introduced into the comb-type electrical cell and oriented parallel and perpendicular to the directions of the applied DC E-field ($40\ \text{V}\ \mu\text{m}^{-1}$) and AC E-field (square wave, $10\ \text{kHz}$, $24\ \text{V}\ \mu\text{m}^{-1}$), respectively. **e**, **g** The sample was introduced into the comb-type electrical cell and subjected to a DC E-field ($40\ \text{V}\ \mu\text{m}^{-1}$) upon cooling at $1\ ^\circ\text{C}\ \text{min}^{-1}$ from its isotropic phase. **f**, **h** The sample was sandwiched by CaF_2 plates and placed in a $9\ \text{T}$ magnetic field upon cooling at $1\ ^\circ\text{C}$

min^{-1} from its isotropic phase. **c**, **d**, **g**, **h** Polarized FT-IR absorption intensities due to H-bonded N–H ($3239\ \text{cm}^{-1}$; purple), $\text{C}\equiv\text{N}$ ($2224\ \text{cm}^{-1}$; orange), N–O• ($1363\ \text{cm}^{-1}$; red), and aryl C–O ($1249\ \text{cm}^{-1}$; light green) were plotted at every 5° interval and were normalized relative to each corresponding minimum value. A_{rel} is the relative absorbance. **i**, **j** Energy diagrams for the electrical reconstruction of columnar LC materials. **i** The noncovalent core-shell column bears an intermediate state featuring disassembled core and shell modules, which **j** the covalent column lacks. **a–d**, **i**, **j**, **e–h** are reproduced from [37] (Copyright: 2019 The American Association for the Advancement of Science) and [40] (Copyright: 2019 American Chemical Society), respectively, with permission

columnar axis (Fig. 6c, d). This unique orientation of the polar functional groups led to the emergence of the dual frequency response of the LC material, the macroscopic orientation of which can be controlled in different directions at two different frequencies (Fig. 6b). This dual frequency response function is often reported for nematic LC materials [39] but has not been reported for columnar LCs before our study. We introduced $^{\text{oCBT}}\text{A}^*\text{-5OCB}$ (molar ratio = 1/6) into an electrical cell with a comb-type electrode and applied a direct current (DC) E-field ($40\ \text{V}\ \mu\text{m}^{-1}$) at $100\ ^\circ\text{C}$

(Fig. 6a, b). The synchrotron 2D X-ray diffraction profile showed two clear diffraction arcs only in the equatorial direction [37]. This indicates that the LC columns are oriented parallel to the applied DC E-field. Polar plots of the polarized infrared (IR) absorption intensities arising from the hydrogen-bonded (H-bonded) amide N–H ($3239\ \text{cm}^{-1}$) and $\text{C}\equiv\text{N}$ ($2224\ \text{cm}^{-1}$) groups showed that the N–H and $\text{C}\equiv\text{N}$ groups preferentially align parallel and perpendicular to the applied E-field. On the other hand, when the applied E-field was switched from DC to AC ($10\ \text{kHz}$, $24\ \text{V}\ \mu\text{m}^{-1}$) at

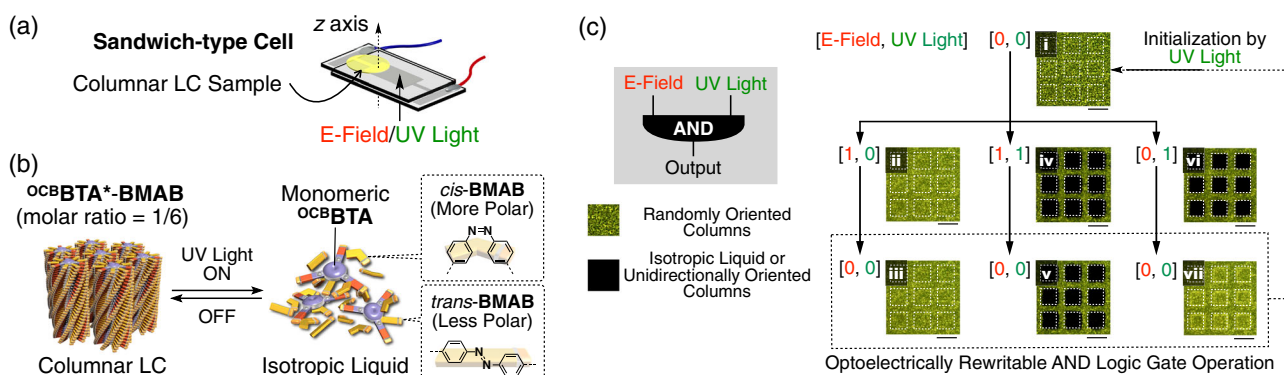


Fig. 7 **a** Schematic representation of a sandwich-type glass cell comprising two parallel glass plates ($5\ \mu\text{m}$ of separation) for vertical E-field application and UV light irradiation. **b** Schematic representations of the photoinduced depolymerization and repolymerization of $\text{OCBTA}^*\text{-BMAB}$ (molar ratio = 1/6) between the columnar LC and its isotropic liquid upon UV light irradiation (365 nm) and backward thermal relaxation. **c** POM images of $\text{OCBTA}^*\text{-BMAB}$ (molar

ratio = 1/6) upon application of a power-tuned DC E-field ($5\ \text{V}\ \mu\text{m}^{-1}$) and/or upon irradiation with 365 nm UV light with a lattice-patterned photomask. Dashed squares represent areas exposed to UV light, whereas the entire area was exposed to the E-field. Scale bars represent $200\ \mu\text{m}$. Reproduced from [37] with permission (Copyright: 2019 The American Association for the Advancement of Science)

$100\ ^\circ\text{C}$, the orientation of the LC columns changed from parallel to perpendicular relative to the applied E-field. The orientation of the N–H and $\text{C}\equiv\text{N}$ groups also changed accordingly (Fig. 6c, d). Importantly, orientation switching can be achieved isothermally through electrical reconstruction, in which electrical disassembly and subsequent assembly of the core-shell columns occur. Generally, isothermal orientation switching of the columns in columnar LCs is difficult due to their high structural integrity, which leads to a high energy barrier for reorientation (Fig. 6j). However, our hybrid columnar LC system can entropically lower the energy barrier by the disassembly of OCBTA and **5OCB** (Fig. 6i). Thus, our hybrid columnar LCs exhibit high levels of structural integrity and stimuli responsiveness, which are mutually exclusive.

The hybrid system exhibits several merits, as it confers a stimuli responsiveness to structurally rigid columnar LCs; in addition, various functions can easily be accommodated with the columnar LCs just by mixing the components. For example, the azobenzene-based rod-shaped nematic LC molecule 4-butyl-4'-methoxy azobenzene (**BMAB**) can be used instead of **5OCB** to give a core-shell columnar LC (Fig. 5d, e). When OCBTA and **BMAB** were mixed in a molar ratio of 1/6, they showed a columnar rectangular LC phase at $140\ ^\circ\text{C}$. Interestingly, even though the molecular structure of **BMAB** does not match with the terminal unit of OCBTA , they can be integrated to form a columnar LC phase without macroscopic phase separation, demonstrating the flexibility of the hybrid columnar LC system. Since **BMAB** undergoes photoisomerization and OCBTA has E-field responsiveness, this hybrid system $\text{OCBTA}\text{-BMAB}$ exhibits both E-field and photoresponsiveness. For the investigation of the E-field and photoresponsiveness, we introduced the LC sample $\text{OCBTA}\text{-BMAB}$ (molar ratio = 1/6) into a

sandwich-type electrical cell partly covered with ITO (Fig. 7a). Under a polarized optical microscope (POM), the LC material exhibited a fan-shaped texture typical of columnar LCs (Fig. 5e). When a voltage of $20\ \text{V}\ \mu\text{m}^{-1}$ was applied to the sample at $140\ ^\circ\text{C}$, the fan-shaped texture in the E-field-exposed area gradually disappeared and became entirely nonbirefringent [37]. This indicates that the columns are aligned perpendicular to the substrate (homeotropic alignment). On the other hand, when a 365 nm ultraviolet (UV) light was irradiated on the sample in the cell at $140\ ^\circ\text{C}$, a phase transition from a columnar LC phase to an isotropic melt occurred and generated a dark image under POM [37]. By taking advantage of this dual responsiveness (E-field and light), we fabricated an LC-based rewritable “AND” logic gate (Fig. 7c). For this purpose, an E-field of $5\ \text{V}\ \mu\text{m}^{-1}$ was utilized, which is too weak to align the LC columns isothermally but can assist the alignment of the columns during the reassembly process from the isotropic melt. When this voltage was applied to the sample, no change in the texture was observed under POM (Fig. 7c, ii, iii). When a 365 nm UV light is applied to a selected area of the sample, they once turned dark but immediately became birefringent once the light was turned off (Fig. 7c, vi, vii). Then, when an E-field and light were applied, the selected area remained dark even after the input signal was removed (Fig. 7c, iv, v). This operation is called the “AND” logic gate. Importantly, the material can be initialized by irradiating the whole area with UV light (Fig. 7c, i).

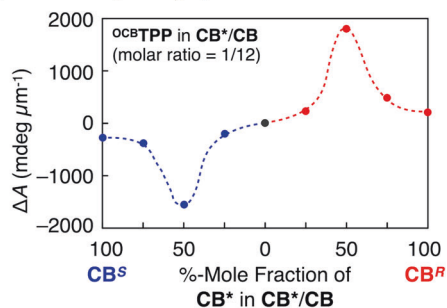
To investigate the flexibility of the disk-shaped molecule, we synthesized NOBTA bearing a bulky organic radical, 2,2,6,6-tetramethylpiperidine 1-oxyl (TEMPO) (Fig. 1) [40]. Usually, such bulky spherical molecular units are incompatible with disk- or rod-shaped molecules due to the mismatch in their assembling preference. However, our

hybrid columnar LC system is flexible enough to accommodate such bulky units. Although NOBTA was a viscous liquid by itself, a mixture of NOBTA and 5OCB in a molar ratio of 1/3 exhibited a hexagonal columnar LC phase at 110 °C (Fig. 5g, h). Interestingly, the structural order of the NOBTA-5OCB system ($p6mm$ symmetry) is higher than that of the $\text{OCB}^{\text{BTA-5OCB}}$ or $\text{OCB}^{\text{BTA-BMAB}}$ system ($c2mm$ symmetry). Therefore, the NOBTA-5OCB system is less prone to be oriented by the E-field. When the sample was subjected to an in-plane E-field of $40 \text{ V } \mu\text{m}^{-1}$ in its mesophase temperature range at 110 °C using a comb-type electrode, the texture under POM remained unchanged [40]. This is in sharp contrast to the previous $\text{OCB}^{\text{BTA-5OCB}}$ system, which can be oriented isothermally [37]. However, when the E-field was applied during the cooling process ($1 \text{ } ^\circ\text{C min}^{-1}$) from its isotropic melt, the columnar mesophase was unidirectionally ordered, as confirmed by the POM texture, which showed bright- and dark-field images alternately every 45° [40], as well as by the polarized FT-IR spectral profile (Fig. 6g). Notably, NOBTA-5OCB (molar ratio = 1/3) could be aligned by a magnetic field. When the sample was sandwiched by calcium fluoride plates and cooled from its isotropic melt to 110 °C at the rate of $1 \text{ } ^\circ\text{C min}^{-1}$ under a 9 T magnetic field, the resultant columnar LC material exhibited a dichroic feature in POM [40] and polarized FT-IR (Fig. 6h). In contrast, the $\text{OCB}^{\text{BTA-5OCB}}$ system was not aligned by a magnetic field. This indicates that the magnetic-field response was conferred by the TEMPO moiety. However, based on electron paramagnetic resonance (EPR) spectral measurements and magnetic susceptibility measurements, NOBTA-5OCB (molar ratio = 1/3) did not show a sign [40] of a magneto-LC effect [41–46]. The observed magnetic-field alignment might be due to the effect of the bulkiness of the TEMPO group, which makes the LC more mobile. This is the first example of a columnar LC material that is responsive to an E-field and magnetic field.

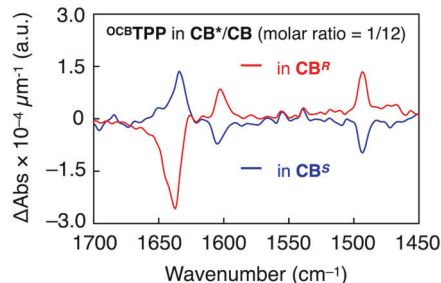
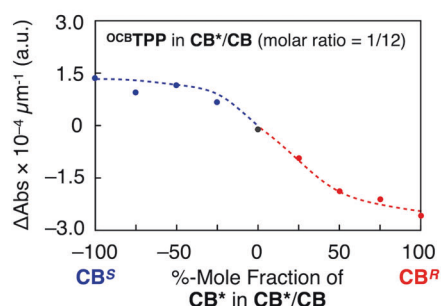
One important aspect of this hybrid columnar LC system is the molecular-level mixing of the shape-incompatible molecules. By means of circular dichroism (CD) spectroscopy, we clarified that the helicity of the supramolecular polymer is transferred to the chiral arrangement of the rod-shaped molecules and vice versa. In the case of $\text{OCB}^{\text{BTA-5OCB}}$ (molar ratio = 1/6), the CD spectra of the disk-shaped molecule and its helical polymer mostly overlap with that of 5OCB , and thus, the relationship between the helical ordering of the two components was difficult to investigate (Fig. 5c). On the other hand, for $\text{OCB}^{\text{BTA-BMAB}}$ (molar ratio = 1/6), the chromophores of OCB^{BTA} and BMAB have different absorption bands, and thus, the chiral ordering of each component can be investigated (Fig. 5f). The CD spectra of $\text{OCB}^{\text{BTA-BMAB}}$ (molar ratio = 1/6) at 140 °C showed distinct bands originating not only from the OCB moiety

(320 nm) but also from BMAB (370 nm) (Fig. 5f). This indicates that the core and shell parts are helically assembled within the column. As for BMAB , NOBTA-5OCB (molar ratio = 1/3) was optically active in the absorption range of the OCB moiety (320 nm) and TEMPO ($\sim 500 \text{ nm}$) (Fig. 5i). This indicates that the radical moiety is in close vicinity to the helical core. These observations clearly demonstrate that the helical arrangement of the disk-shaped molecules is successfully transferred to the arrangement of the rod-shaped molecules.

Here one question arose; can the chirality of the shell part consisting of rod-shaped molecules be transferred to the helicity of the core part consisting of disk-shaped molecules? To explore this possibility, we designed a new achiral H-bonding disk-shaped molecule, OCB^{TPP} , which has a tetraphenyl porphyrin (TPP) core appended with four OCB-terminated achiral side chains (Fig. 1) [47]. In the previous design using BTA, the electronic absorption and CD spectral bands for the OCB unit and BTA unit overlapped with each other, and thus, it was difficult to investigate the chiral transfer from the shell to the core. Through the new molecule OCB^{TPP} , we could observe the spectral bands separately between the OCB unit and TPP unit due to the large difference in the absorption range. For a rod-shaped molecule, we employed 4-cyano-4'-(2-methylbutyl) biphenyl (CB^*), which has a chiral center on its C5 side chain (Fig. 1). This molecule was reported to show a smectic A phase at $> -54 \text{ } ^\circ\text{C}$ and a cholesteric phase at $-54 \sim -30 \text{ } ^\circ\text{C}$ [48]. As for the above examples, $\text{OCB}^{\text{TPP-CB}^*}$ (molar ratio = 1/12) exhibited a columnar phase ($p2$ oblique lattice) below 48 °C (Fig. 5j, k). Interestingly, the CD spectral profile clearly exhibited a bisignate Cotton effect at 400–450 nm, which corresponds to the Soret band due to the porphyrin core (Fig. 5l). This clearly indicates that chiral transfer from the shell to the core took place. Therefore, the helical core and the shell exhibit a strong interaction to affect the molecular arrangement. More interestingly, we found an anomalous relationship between the degree of chirality of the rod-shaped molecule and the CD intensity. When the difference between the peak top CD intensity values of positive and negative Cotton effects ($|A|$) was calculated and plotted as a function of the %-enantiomeric excess (%*ee*) of CB^* , the plot showed a sigmoidal curve [47]. Such a nonlinear relationship is known as the “majority rule”, which is often observed in the supramolecular polymerization of chiral monomers in an achiral solvent [49, 50]. In supramolecular polymerization, a similar relationship called the “sergeant and soldier principle” is also known, in which the incorporation of a chiral monomer into the supramolecular polymer of an achiral monomer can sigmoidally increase the CD intensity [5, 51–54]. However, when we utilized a mixture of chiral CB^* and achiral 5-cyanobiphenyl CB as a rod-shaped component and varied the %-mole fraction of CB^* in CB^*/CB (χ), an anomalous bell-shaped relationship was observed (Fig. 8a). The maximum CD intensity reached $1800 \text{ mdeg } \mu\text{m}^{-1}$

(a) CD intensity change profile at various CB^*/CB ratio

(b)

(c) VCD intensity change profile at various CB^*/CB ratio

(d)

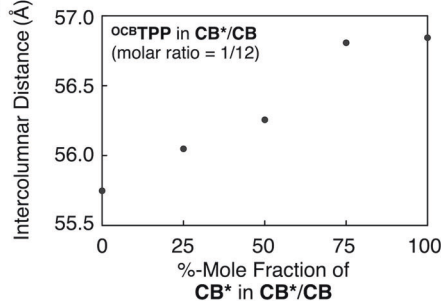


Fig. 8 **a** ΔA values of OCB^{TPP} (molar ratio = 1/12) in $\text{CB}^{\text{R}}_{100}/\text{CB}_0$, $\text{CB}^{\text{R}}_{75}/\text{CB}_{25}$, $\text{CB}^{\text{R}}_{50}/\text{CB}_{50}$, $\text{CB}^{\text{R}}_{25}/\text{CB}_{75}$ (red circles), CB (black circle), $\text{CB}^{\text{S}}_{25}/\text{CB}_{75}$, $\text{CB}^{\text{S}}_{50}/\text{CB}_{50}$, $\text{CB}^{\text{S}}_{75}/\text{CB}_{25}$, $\text{CB}^{\text{S}}_{100}/\text{CB}_0$ (blue circles) at 40 °C. **b** VCD spectra of OCB^{TPP} in $\text{CB}^{\text{R}}/\text{CB}$ (molar ratio = 1/12) (red trace) and OCB^{TPP} in $\text{CB}^{\text{S}}/\text{CB}$ (molar ratio = 1/12) (blue trace) at 30 °C. **c** VCD peak top signal intensities that correspond to the C=O stretching vibration ($\sim 1638 \text{ cm}^{-1}$) of OCB^{TPP} (molar ratio = 1/12) in $\text{CB}^{\text{R}}_{100}/\text{CB}_0$, $\text{CB}^{\text{R}}_{75}/\text{CB}_{25}$, $\text{CB}^{\text{R}}_{50}/\text{CB}_{50}$, $\text{CB}^{\text{R}}_{25}/\text{CB}_{75}$ (red circles), CB (black circle), $\text{CB}^{\text{S}}_{25}/\text{CB}_{75}$, $\text{CB}^{\text{S}}_{50}/\text{CB}_{50}$, $\text{CB}^{\text{S}}_{75}/\text{CB}_{25}$, and $\text{CB}^{\text{S}}_{100}/\text{CB}_0$ (blue circles). **d** Intercolumnar distances of OCB^{TPP} in CB^*/CB (molar ratio = 1/12) at various % mole fractions of CB^* at 40 °C. Reproduced from [47] with permission (Copyright: 2022 Wiley-VCH)

at $\chi = 50\%$. This corresponds to the anisotropic dissymmetry factor g_{abs} of 0.049 ($\lambda = 441 \text{ nm}$), which is the highest value among all reported helical supramolecular polymers [5, 53, 54] as well as columnar LCs [55, 56]. Interestingly, the vibrational circular dichroism (VCD) spectroscopy of the same sample set gave an ordinary sigmoidal relationship between the χ value and the intensity of the VCD band (Δ_{abs}) (Fig. 8b,c). This is similar to the typical “sergeant-soldier principle” [5, 51–54]. These results indicate that the anomalous nonlinear relationship observed for CD intensity is not due to the enhanced helical induction but the change in the spatial relationship between the chromophores. The detailed investigation between the intercolumnar distance and χ revealed that the intercolumnar distance decreased upon increasing the achiral component (Fig. 8d). Considering that the shape and intensity of the CD spectrum are highly sensitive to the stacking manner of chromophores [57, 58], the anomalous trend in the CD intensity is likely due to the change in the stacking manner of the porphyrin units caused by the change in the intercolumnar interaction. Namely, the enhancement in the CD intensity from $\chi = 100$ to 50% is due to the change in the stacking manner of the chromophores by the increased intercolumnar interaction, and the subsequent CD intensity drop is due to the decrease in the chiral component in the material.

Summary and perspective

In this Focus Review, we summarized our new concept of electroresponsive dopants to construct novel electroresponsive soft materials. The dopants we designed respond to electrical stimuli in different ways. The one used for the cholesteric display bearing a rewritable color memory function ($^{\text{Ion}}\text{D}$) responds to an E-field to undergo electrophoretic deposition and change its concentration in the LC material. On the other hand, the one used for the cholesteric display with a quick color modulation function ($^{\text{Fc}}\text{D}$) undergoes a redox reaction to change its ionicity and eventually changes its HTP value. The disk-shaped supramolecularly polymerizable dopants ($^{\text{OCB}}\text{BTA}$, $^{\text{NO}}\text{BTA}$) not only function as a property-changing molecule but also as a structure-transforming agent to a higher-order molecular ordering of the system. The response of those dopants is not the response of the individual molecules but rather their polymerized 1D architecture, in which they can change their orientation depending on the direction and the frequency of the E-field. The dopant concentration we employed was below 15 mol%. This value could be lowered more by an appropriate molecular design. Our study demonstrates that modifying the constituent molecule of such a small amount can drastically change the properties of the host materials.

This is an efficient way to confer stimuli-responsiveness to a material, allowing facile material design and energy-efficient function. One interesting perspective is to design a dopant that can operate within a lyotropic liquid crystal phase. By doing so, a material could be designed that can operate in a biological system, such as a cell membrane, with a minimum amount of dopant molecules.

Thus far, LC materials have created an era through their application to display devices. The exploration of new possibilities for LC materials is currently active. We hope that our work will help reveal a new direction for next-generation LC materials.

Acknowledgements The author acknowledges all the collaborators who contributed to the research projects described in this article. This work was financially supported by a JSPS Grant-in-Aid for Challenging Exploratory Research (16K14062), Young Scientists (A) (16H06035), Scientific Research (B) (21H01903), and JST, PRESTO grant JPMJPR21Q1.

Funding Open access funding provided by The University of Tokyo.

Compliance with ethical standards

Conflict of interest The authors declare no competing interests.

Publisher's note Springer Nature remains neutral with regard to jurisdictional claims in published maps and institutional affiliations.

Open Access This article is licensed under a Creative Commons Attribution 4.0 International License, which permits use, sharing, adaptation, distribution and reproduction in any medium or format, as long as you give appropriate credit to the original author(s) and the source, provide a link to the Creative Commons license, and indicate if changes were made. The images or other third party material in this article are included in the article's Creative Commons license, unless indicated otherwise in a credit line to the material. If material is not included in the article's Creative Commons license and your intended use is not permitted by statutory regulation or exceeds the permitted use, you will need to obtain permission directly from the copyright holder. To view a copy of this license, visit <http://creativecommons.org/licenses/by/4.0/>.

References

- de Gennes PG, Prost J. The physics of liquid crystals. New York: Oxford University Press; 1995.
- Yang DK, Wu ST. Fundamentals of liquid crystal devices. 2nd ed. Chichester: John Wiley & Sons; 2014.
- Schadt M. Liquid crystal materials and liquid crystal displays. *Annu Rev Mater Sci.* 1997;27:305–79.
- Chen H-W, Lee J-H, Lin B-Y, Chen S, Wu S-T. Liquid crystal display and organic light-emitting diode display: present status and future perspectives. *Light Sci Appl.* 2018;7:17168.
- Palmans ARA, Meijer EW. Amplification of chirality in dynamic supramolecular aggregates. *Angew Chem Int Ed.* 2007;46:8948–68.
- Pieraccini S, Masiero S, Ferrarini A, Spada GP. Chirality transfer across length-scales in nematic liquid crystals: fundamentals and applications. *Chem Soc Rev.* 2010;40:258–71.
- Reinitzer F. Beiträge zur kenntniss des cholesterins. *Monatsh Chem.* 1888;9:421–41.
- Reinitzer F. Contributions to the knowledge of cholesterol. *Liq Cryst.* 1989;5:7–18.
- White TJ, McConney ME, Bunning TJ. Dynamic color in stimuli-responsive cholesteric liquid crystals. *J Mater Chem.* 2010;20:9832–47.
- Hikmet RAM, Kemperman H. Electrically switchable mirrors and optical components made from liquid-crystal gels. *Nature.* 1998;392:476–9.
- Pasechnik S, Chigrinov V, Shmeliova D. Liquid crystals. Berlin: Wiley; 2009.
- Wu ST, Yang DK. Reflective liquid crystal displays. Chichester: Wiley; 2001.
- Xianyu H, Faris S, Crawford GP. In-plane switching of cholesteric liquid crystals for visible and near-infrared applications. *Appl Opt.* 2004;43:5006–15.
- Lin T-H, Jau H-C, Chen C-H, Chen Y-J, Wei T-H, Chen C-W, et al. Electrically controllable laser based on cholesteric liquid crystal with negative dielectric anisotropy. *Appl Phys Lett.* 2006;88:061122.
- Bailey CA, Tondiglia VP, Natarajan LV, Duning MM, Bricker RL, Sutherland RL, et al. Electromechanical tuning of cholesteric liquid crystals. *J Appl Phys.* 2010;107:013105.
- Choi SS, Morris SM, Coles HJ, Huck WTS. Wavelength tuning the photonic band gap in chiral nematic liquid crystals using electrically commanded surfaces. *Appl Phys Lett.* 2007;91:231110.
- Choi SS, Morris SM, Huck WTS, Coles HJ. The switching properties of chiral nematic liquid crystals using electrically commanded surfaces. *Soft Matter.* 2009;5:354–62.
- Choi SS, Morris SM, Huck WTS, Coles HJ. Electrically tuneable liquid crystal photonic bandgaps. *Adv Mater.* 2009;21:3915–8.
- Tokunaga S, Itoh Y, Yaguchi Y, Tanaka H, Araoka F, Takezoe H, et al. Electrophoretic deposition for cholesteric liquid-crystalline devices with memory and modulation of reflection colors. *Adv Mater.* 2016;28:4077–83.
- Tokunaga S, Itoh Y, Tanaka H, Araoka F, Aida T. Redox-responsive chiral dopant for quick electrochemical color modulation of cholesteric liquid crystal. *J Am Chem Soc.* 2018;140:10946–9.
- Han Y, Pacheco K, Bastiaansen CWM, Broer DJ, Sijbesma RP. Optical monitoring of gases with cholesteric liquid crystals. *J Am Chem Soc.* 2010;132:2961–7.
- Wang L, Li Q. Stimuli-directing self-organized 3D liquid-crystalline nanostructures: from materials design to photonic applications. *Adv Funct Mater.* 2016;26:10–28.
- Wang Y, Li Q. Light-driven chiral molecular switches or motors in liquid crystals. *Adv Mater.* 2012;24:1926–45.
- van Delden RA, Koumura N, Harada N, Feringa BL. Unidirectional rotary motion in a liquid crystalline environment: color tuning by a molecular motor. *Proc Natl Acad Sci USA.* 2002;99:4945–9.
- Mathews M, Tamaoki N. Planar chiral azobenzenophanes as chiroptic switches for photon mode reversible reflection color control in induced chiral nematic liquid crystals. *J Am Chem Soc.* 2008;130:11409–16.
- Wang L, Dong H, Li Y, Liu R, Wang Y-F, Bisoyi HK, et al. Luminescence-driven reversible handedness inversion of self-organized helical superstructures enabled by a novel near-infrared light nanotransducer. *Adv Mater.* 2015;27:2065–9.
- Wang L, Dong H, Li Y, Xue C, Sun L-D, Yan C-H, et al. Reversible near-infrared light directed reflection in a self-organized helical superstructure loaded with upconversion nanoparticles. *J Am Chem Soc.* 2014;136:4480–3.
- Bisoyi HK, Li Q. Light-directing chiral liquid crystal nanostructures: from 1D to 3D. *Acc Chem Res.* 2014;47:3184–95.
- Wang L, Chen D, Gutierrez-Cuevas KG, Bisoyi HK, Fan J, Zola RS, et al. Optically reconfigurable chiral microspheres of

- self-organized helical superstructures with handedness inversion. *Mater Horiz*. 2017;4:1190–5.
30. Zheng Z, Li Y, Bisoyi HK, Wang L, Bunning TJ, Li Q. Three-dimensional control of the helical axis of a chiral nematic liquid crystal by light. *Nature*. 2016;531:352–6.
 31. Bard AJ, Faulkner LR. *Electrochemical methods: fundamentals and applications*. 2nd ed. New Jersey: John Wiley & Sons Inc.; 2001.
 32. Sapp S, Luebben S, Losovyj YAB, Jeppson P, Schulz DL, Caruso AN. Work function and implications of doped poly(3,4-ethylenedioxythiophene)-co-poly(ethylene glycol). *Appl Phys Lett*. 2006;88:152107.
 33. Miyajima D, Araoka F, Takezoe H, Kim J, Kato K, Takata M, et al. Electric-field-responsive handle for large-area orientation of discotic liquid-crystalline molecules in millimeter-thick films. *Angew Chem Int Ed*. 2011;50:7865–9.
 34. Sato K, Itoh Y, Aida T. Columnar assembled liquid-crystalline peptidic macrocycles unidirectionally orientable over a large area by an electric field. *J Am Chem Soc*. 2011;133:13767–9.
 35. Miyajima D, Araoka F, Takezoe H, Kim J, Kato K, Takata M, et al. Ferroelectric columnar liquid crystal featuring confined polar groups within core-shell architecture. *Science*. 2012;336:209–13.
 36. Araoka F, Masuko S, Kogure A, Miyajima D, Aida T, Takezoe H. High-optical-quality ferroelectric film wet-processed from a ferroelectric columnar liquid crystal as observed by non-linear-optical microscopy. *Adv Mater*. 2013;25:4014–7.
 37. Yano K, Itoh Y, Araoka F, Watanabe G, Hikima T, Aida T. Nematic-to-columnar mesophase transition by in situ supramolecular polymerization. *Science*. 2019;363:161–5.
 38. Kato T, Hirai Y, Nakaso S, Moriyama M. Liquid-crystalline physical gels. *Chem Soc Rev*. 2007;36:1857–67.
 39. Xianyu H, Wu S-T, Lin C-L. Dual frequency liquid crystals: a review. *Liq Cryst*. 2009;36:717–26.
 40. Yano K, Hanebuchi T, Zhang X-J, Itoh Y, Uchida Y, Sato T, et al. Supramolecular polymerization in liquid crystalline media: toward modular synthesis of multifunctional core-shell columnar liquid crystals. *J Am Chem Soc*. 2019;141:10033–8.
 41. Uchida Y, Ikuma N, Tamura R, Shimono S, Noda Y, Yamauchi J, et al. Unusual intermolecular magnetic interaction observed in an all-organic radical liquid crystal. *J Mater Chem*. 2008;18:2950–2.
 42. Uchida Y, Tamura R, Ikuma N, Shimono S, Yamauchi J, Shimbo Y, et al. Magnetic-field-induced molecular alignment in an achiral liquid crystal spin-labeled by a nitroxyl group in the mesogen core. *J Mater Chem*. 2009;19:415–8.
 43. Uchida Y, Suzuki K, Tamura R, Ikuma N, Shimono S, Noda Y, et al. Anisotropic and inhomogeneous magnetic interactions observed in all-organic nitroxide radical liquid crystals. *J Am Chem Soc*. 2010;132:9746–52.
 44. Uchida Y, Suzuki K, Tamura R. Magneto-LC effects in hydrogen-bonded all-organic radical liquid crystal. *J Phys Chem B*. 2012;116:9791–5.
 45. Tamura R, Uchida Y, Suzuki K. Magnetic properties of organic radical liquid crystals and metallomesogens. In: Goodby JW, Collings PJ, Kato T, et al., editors. *Handbook of liquid crystals*. Vol. 8. Weinheim: Wiley-VCH; 2014. p. 837–64.
 46. Akita T, Sugiyama Y, Yamazaki T, Nakagami S, Kiyohara D, Uchida Y, et al. Photomagnetic effects in metal-free liquid crystals. *Commun Chem*. 2019;2:1–8.
 47. Zhang X-J, Morishita D, Aoki T, Itoh Y, Yano K, Araoka F, et al. Anomalous chiral transfer: supramolecular polymerization in a chiral medium of a mesogenic molecule. *Chem Asian J*. 2022;17:e202200223.
 48. Gray GW, McDonnell DG. Synthesis and liquid crystal properties of chiral alkyl-cyano-biphenyls (and -p-Terphenyls) and of some related chiral compounds derived from biphenyl. *Mol Cryst Liq Cryst*. 1976;37:189–211.
 49. van Gestel J, Palmans ARA, Titulaer B, Vekemans JAJM, Meijer EW. “Majority-rules” operative in chiral columnar stacks of C3-symmetrical molecules. *J Am Chem Soc*. 2005;127:5490–4.
 50. Jin W, Fukushima T, Niki M, Kosaka A, Ishii N, Aida T. Self-assembled graphitic nanotubes with one-handed helical arrays of a chiral amphiphilic molecular graphene. *Proc Natl Acad Sci USA*. 2005;102:10801–6.
 51. Palmans ARA, Vekemans JAJM, Havinga EE, Meijer EW. Sergeants-and-soldiers principle in chiral columnar stacks of disc-shaped molecules with C3 symmetry. *Angew Chem Int Ed*. 1997;36:2648–51.
 52. Kim T, Mori T, Aida T, Miyajima D. Dynamic propeller conformation for the unprecedentedly high degree of chiral amplification of supramolecular helices. *Chem Sci*. 2016;7:6689–94.
 53. Yashima E, Ousaka N, Taura D, Shimomura K, Ikai T, Maeda K. Supramolecular helical systems: helical assemblies of small molecules, foldamers, and polymers with chiral amplification and their functions. *Chem Rev*. 2016;116:13752–990.
 54. Hembury GA, Borovkov VV, Inoue Y. Chirality-sensing supramolecular systems. *Chem Rev*. 2008;108:1–73.
 55. Nuckolls C, Katz TJ. Synthesis, structure, and properties of a helical columnar liquid crystal. *J Am Chem Soc*. 1998;120:9541–4.
 56. Hu J, Zhu T, He C, Zhang Y, Zhang Q, Zou G. Chiral induction, transfer and modulation in C3-symmetric columnar liquid crystalline assemblies. *J Mater Chem C*. 2017;5:5135–42.
 57. Berova N, Bari LD, Pescitelli G. Application of electronic circular dichroism in configurational and conformational analysis of organic compounds. *Chem Soc Rev*. 2007;36:914–31.
 58. Pescitelli G, Bari LD, Berova N. Conformational aspects in the studies of organic compounds by electronic circular dichroism. *Chem Soc Rev*. 2011;40:4603–25.



Dr. Yoshimitsu Itoh received a Ph.D. degree for experimental and theoretical investigations of organo-fluorine compounds under the direction of Prof. Koichi Mikami at Tokyo Institute of Technology in 2006. Then, he started his first postdoctoral research focusing on organometallic catalysis with Prof. Eiichi Nakamura at the University of Tokyo. His second postdoctoral research was completed at Columbia University starting from 2007 with Prof. Colin Nuckolls working on self-assembled monolayers and organic field effect transistors. In 2008, he began his academic career at the University of Tokyo as an assistant professor in Prof. Takuzo Aida's group. He was promoted to Lecturer in 2016 and then to Associate Professor in 2018. In 2022, he successfully started his independent lab named Interfacial Molecular Engineering Lab. His current research interest is to engineer the interface between molecules, and between molecules and surfaces to develop innovative materials based on organic chemistry, polymer chemistry, supramolecular chemistry, and electrochemistry.



Daiki Morishita received his B.A. with a major in chemistry from International Christian University in 2019 under the supervision of Prof. Julian R. Koe, and his M.Eng. from the University of Tokyo in 2021 under the supervision of Prof. Takuzo Aida. He is currently pursuing his Ph.D. under the supervision of Prof. Yoshimitsu Itoh, sponsored by the University Fellowship Founding Project for Innovation Creation in Science and Technology, “Fellowship for Integrated Materials Science and Career Development”. His current research interests include molecular self-assembly and structural organic chemistry.